American Mineralogist, Volume 71, pages 937–945, 1986

Phase transitions in leucite ($KAlSi_2O_6$), orthorhombic $KAlSiO_4$, and their iron analogues ($KFeSi_2O_6$, $KFeSiO_4$)

REBECCA A. LANGE, IAN S. E. CARMICHAEL
Department of Geology and Geophysics, University of California, Berkeley, Berkeley, California 94720
JONATHAN F. STEBBINS
Earth Sciences Division, Lawrence Berkeley Laboratory, Berkeley, California 94720

ABSTRACT

The heat capacities of natural and synthetic samples of leucite ($KAlSi_2O_6$), orthorhombic $KAlSiO_4$, and their iron analogues, $KFeSi_2O_6$ and $KFeSiO_4$, have been measured between 400 and 1000 K by differential scanning calorimetry. For the various phase transitions that occur, temperatures of transition and associated changes in enthalpy and entropy have been determined. The tetragonal–cubic transition in leucite spans 122 to 176 deg, depending upon the sample studied, and is characterized by two peaks on a C_P heating curve. Heat treatment of a natural leucite for one week at 1673 K lowers the transition by 24 deg. Two distinct peaks in the C_P curve, enhanced by heating, suggest that an intermediate phase exists that is stable over 17 deg. A space group of $I4_1/acd$ has been assigned to this phase because it can be related to the low-temperature tetragonal leucite phase ($I4_1/a$) by merohedric twinning and the high-temperature cubic leucite phase ($Ia3d$) by pseudomerohedric twinning, both of which are found in leucite. In contrast, $KFeSi_2O_6$ (leucite structure) has a single, sharp C_P peak at a lower transition temperature. A natural leucite consisting of 88 wt% $KAlSi_2O_6$ and 12 wt% $KAlSi_3O_8$ has an X-ray pattern that indicates tetragonal symmetry, yet appears to be without twinning when viewed optically. The C_P data indicate a very small transition effect which may, however, be spread out in temperature above the limit of the DSC (1000 K). The orthorhombic polymorph of $KAlSiO_4$ undergoes one transition at 695 and one at 817 K, whereas its iron analogue, orthorhombic $KFeSiO_4$, has a single transition at 729.5 K. The enthalpy and entropy data indicate that the single transition in orthorhombic $KFeSiO_4$ is approximately equivalent to the sum of the two transitions in $KAlSiO_4$.

INTRODUCTION

Many tectosilicate minerals, such as tridymite (SiO_2), pure-Na nepheline ($NaAlSiO_4$), leucite ($KAlSi_2O_6$), and orthorhombic $KAlSiO_4$, have high-order phase changes that are affected by composition, ordering state, and crystal structure. To understand transition mechanisms and to calculate high-temperature phase equilibria, the energetics of these transitions must be known. Currently, limited information exists on the thermodynamic properties of the various feldspathoid minerals. The best-studied minerals in terms of calorimetric data are nepheline [(K, Na)$AlSiO_4$] and tridymite (Henderson and Thompson, 1980; Thompson and Wennemer, 1979), which are both characterized by multiple transitions below 700 K. On the potassic side of the nepheline-kalsilite join, enthalpy and heat-capacity data exist for only one phase, kaliophilite (Pankratz, 1968), although several polymorphs are known (Smith and Tuttle, 1957; Cook et al., 1977; Abbott, 1984). Heat capacities for synthetic leucite have been measured (Pankratz, 1968), but data on natural samples, $KFeSi_2O_6$ (leucite structure), and SiO_2-rich leucite are lacking.

Leucite is a characteristic mineral of K-rich, SiO_2-poor lavas. At high temperatures it has cubic symmetry, but during cooling it reversibly changes to a tetragonal form. The transition involves a collapse of the (Si,Al)–O framework about the K cations and two types of complex, repeated twinning on the {110} crystallographic planes: merohedric and pseudomerohedric (Mazzi et al., 1976). Thermal-expansion data (Taylor and Henderson, 1968; Hirao et al., 1976) in conjunction with heat-content measurements (Pankratz, 1968) indicate that the tetragonal–cubic transition is continuous, displacive, and second order. DTA (differential thermal analysis) heating curves for natural and synthetic leucites (Faust, 1963) show that the transition is characterized by two endothermic peaks with a positive hysteresis (i.e., the transition occurs at lower temperatures during cooling than during heating). However, when Fe^{3+} substitutes for Al, $KFeSi_2O_6$ has a single, sharp DTA peak at a lower temperature.

Two hexagonal polymorphs of $KAlSiO_4$ also occur in K-rich, volcanic rocks: kalsilite and, less commonly, kaliophilite (Bannister, 1931; Holmes, 1942). Pankratz (1968) conducted drop calorimetry experiments on a synthesized

0003–004X/86/0708–0937$02.00

Table 1. Key to specimen numbers

89-21	Natural leucite from leucite-trachyte, Mt. Cimini, Roman District, Italy
89-21-A	Mt. Cimini leucite heated at 1673 K for one week
90-05	Natural leucite from leucite-phonolite, Rocca Monfina, Roman District, Italy
1774	Natural leucite from wyomingite, Leucite Hills, Wyoming, U.S.A.
SL.1	Synthetic leucite ($KAlSi_2O_6$)
FL.1	Synthetic $KFeSi_2O_6$
SL.2	Synthetic solid solution of 86 wt % ($KAlSi_2O_6$) 14 wt % ($KAlSi_3O_8$)
O1	Synthetic orthorhombic $KAlSiO_4$
α−KF	Synthetic orthorhombic $KFeSiO_4$
β−KF	Synthetic hexagonal $KFeSiO_4$

material identified by X-ray data as kaliophilite. A transition near 810 K with an enthalpy of transition of 576 J/mol was described as first order. The kaliophilite was synthesized by Kelley et al. (1953) at 1723 K and 1 atm. However, based on phase-equilibrium studies by Tuttle and Smith (1958) and Cook et al. (1977), such conditions of synthesis should produce the orthorhombic form of $KAlSiO_4$. Perhaps, like nephelines synthesized in the $NaAlSiO_4$-$KAlSiO_4$ system (Henderson and Thompson, 1980), the structure of the various $KAlSiO_4$ polymorphs is critically dependent on the method of synthesis.

To study the effects of cation size and ordering on the phase transitions in leucite and $KAlSiO_4$, heat capacities between 400 and 1000 K for natural and synthetic samples of $KAlSi_2O_6$ and $KAlSiO_4$ and for their iron analogues, $KFeSi_2O_6$ and $KFeSiO_4$, have been measured using a differential scanning calorimeter (DSC). For the various phase transitions that occur, temperatures of transition and associated changes in enthalpy and entropy have been determined. Various structural interpretations of the nature of the tetragonal–cubic transformation in leucite, $KFeSi_2O_6$, and SiO_2-rich leucite, as well as the two transitions in orthorhombic $KAlSiO_4$ vs. the single transition in orthorhombic $KFeSiO_4$, are discussed.

Experimental methods

Composition and synthesis of specimens

The specimen localities of the three natural leucites used in this study are given in Table 1. A portion of the Mt. Cimini leucite (specimen 89-21) was heat treated for one week at 1673 K and labeled 89-21-A. Chemical analyses of the specimens (Table 2) were performed by both electron-microprobe and wet-chemical techniques. The stoichiometry of the wyomingite leucite (specimen 1774) corresponds to a solid solution of 88 wt% $KAlSi_2O_6$ and 12 wt% $KAlSi_3O_8$, in addition to 2.1 wt% Fe_2O_3. Although the wyomingite leucite shows no twinning optically, its X-ray diffraction pattern matches that of the tetragonal form.

Table 2. Chemical analyses of specimens

Sample	89−21[1]	89−21−A[1]	90−05[2]	1774[1]	FL.1[1]	SL.2[2]	O1[2]	α−KF[2]
SiO_2	54.4	54.9	55.2	56.2	48.4	56.6	36.8	32.3
Al_2O_3	22.5	23.0	22.7	20.3	-	23.0	34.9	-
Fe_2O_3	0.3	0.3	0.3	2.1	32.3	0.1	0.1	42.1
Na_2O	0.3	0.3	0.8	-	-	-	-	-
K_2O	20.9	20.0	20.2	21.1	18.9	20.2	27.9	25.1
Total	98.4	98.5	99.2	99.7	99.6	99.3	99.7	99.5
gfw[3]	217.97	216.45	216.63	219.00	247.09	216.01	156.48	186.94

[1]Electron microprobe data (wt %)

[2]Wet chemical data (wt %)

[3]gfw – gram formula weight based on six oxygens for leucites and four oxygens for O1 and α-KF

Synthetic leucite ($KAlSi_2O_6$; specimen SL.1) was prepared hydrothermally from a gel at 1033 K and 1 kbar for 37 h by W. S. MacKenzie. $KFeSi_2O_6$ (leucite structure, specimen FL.1) was synthesized by mixing together appropriate amounts of potassium carbonate, ferric oxide, and dehydrated silicic acid. The mixture was melted at 1573 K and allowed to crystallize for 4 d at 1273 K, then remelted at 1673 K and crystallized for 3 d at 1273 K. Electron-microprobe and wet-chemistry data (Table 2) confirm that the resulting crystalline material consists of the single phase $KFeSi_2O_6$ and that all of the iron is in the ferric state.

A silica-rich sample of leucite (specimen SL.2) was prepared as a gel (Hamilton and Henderson, 1968). The dehydrated gel was loaded into a Pt crucible and heated for 3 d at 1373 K. A portion of the sample was then removed while the rest was heated for another 5 d at 1773 K. Electron-microprobe and wet-chemistry data on the crystalline product (Table 1) indicate that it is a leucite solid solution with approximately 14 wt% of the $KAlSi_3O_8$ component.

The high-temperature $KAlSiO_4$ orthorhombic phase (denoted as O1 after Smith and Tuttle, 1957) was synthesized by mixing together potassium carbonate, aluminum oxide, and dehydrated silicic acid. The sample crystallized for 2 d at 1573 K and for 3 d at 1773 K. To synthesize hexagonal β-$KFeSiO_4$ (isomorphous with kalsilite; Bentzen, 1983) and orthorhombic $KFeSiO_4$ (α-$KFeSiO_4$; Bentzen, 1983), potassium carbonate, ferric oxide, and dehydrated silicic acid were mixed and melted. Half of this melt crystallized for 2 d at 1573 K and 3 d at 1373 K, forming orthorhombic α-$KFeSiO_4$ (denoted as α-KF), while the other half crystallized at 1103 K for 5 d, forming hexagonal β-$KFeSiO_4$ (denoted as β-KF). X-ray data for each of the $KAlSiO_4$ and $KFeSiO_4$ samples were compared to data presented by Smith and Tuttle (1957) and Bentzen (1983).

DSC procedures

Heat-capacity data were collected on each of the specimens described above with a Perkin-Elmer DSC-2 calorimeter. Detailed DSC procedures are given by Stebbins et al. (1982). Each specimen was heated and cooled at a rate of 20 deg/min throughout the temperature range of 400 to 1000 K. The entire temperature range was split into five separate intervals, each spanning approximately 150 deg and overlapping by 20 deg. Each specimen was run three times over each interval alternating with runs on NBS-720 sapphire, but only the last two runs were recorded. Data points were collected every 0.5 deg. Plots of heat capacity as a function of temperature for each sample (Figs. 1, 2) between 400 and 1000 K not only record phase transitions with their associated temperature interval, but also demonstrate the repro-

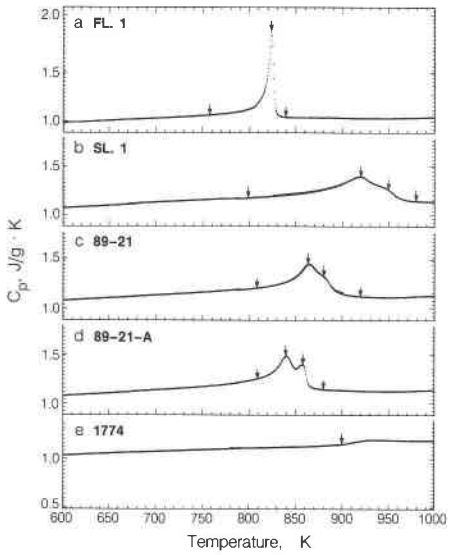

Fig. 1. Heat-capacity data showing phase transitions in five leucite samples: (a) synthetic $KFeSi_2O_6$ (specimen FL.1); (b) synthetic $KAlSi_2O_6$ (specimen SL.1); (c) natural leucite from Mt. Cimini, Italy (specimen 89-21); (d) heat-treated Mt. Cimini leucite (specimen 89-21-A); (e) leucite from a wyomingite lava (specimen 1774). Arrows indicate points on the C_P curve associated with the beginning of the transition, the primary peak, the secondary peak, and the end of the transition (Table 3).

ducibility of the runs. C_P measurements collected several months apart on the same specimen were identical within less than 1% precision.

Heat-capacity data

The tetragonal–cubic transition in leucite takes place over a broad temperature interval spanning 82 to 176 deg, depending upon the sample studied. Figure 1 shows data for five samples: (a) synthetic $KFeSi_2O_6$ (FL.1), (b) synthetic leucite (SL.1); (c) a natural leucite from Mt. Cimini of the Roman volcanic province, Italy (89-21), (d) heat-treated Mt. Cimini leucite (one week at 1673 K, 89-21-A), and (e) leucite from a wyomingite from Leucite Hills, Wyoming (1774). The abrupt phase change in the $KFeSi_2O_6$ contrasts sharply with the broad, double-peaked transitions of the Al analogues. Comparison of the Mt. Cimini leucite (c) to its heat-treated analogue (d) shows that the heat treatment lowered the transition temperature by 24 deg and enhanced the separation of two peaks on the heat-capacity curves. The wyomingite leucite (e) begins to transform at 900 K but continues above the limit of the DSC at 1000 K. These data are from heating experiments, whereas C_P plots from cooling runs are identical with respect to the shape of the transition peaks but show minor hysteresis (Table 3).

Figure 2 is a plot of heat capacity vs. temperature for O1 and orthorhombic $KFeSiO_4$ (α-KF). O1 undergoes a rapid transition at 695 K and another rapid one at 817 K, whereas α-KF has a single transition spread over 180

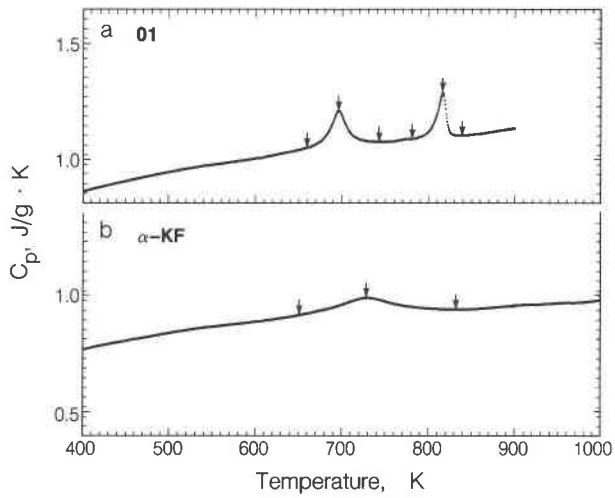

Fig. 2. Heat-capacity data showing phase transitions in (a) O1 and (b) α-KF (orthorhombic $KFeSiO_4$). Arrows point to the beginning, the peak, and the end of each transition.

deg. In contrast to leucite, the effect of Fe^{3+} substitution in O1 is to make the transition broader rather than narrower. The second transition observed for O1 corresponds to the single transition observed by Pankratz (1968) for the polymorph he identified as kaliophilite. The stable, low-temperature polymorph, hexagonal β-$KFeSiO_4$ (β-KF), undergoes no phase transitions below 1000 K.

Table 3 lists transition temperature intervals and temperatures associated with the heat-capacity peaks upon heating and cooling for each of the leucite, $KAlSiO_4$, and $KFeSiO_4$ samples. Figures 1 and 2 illustrate which tem-

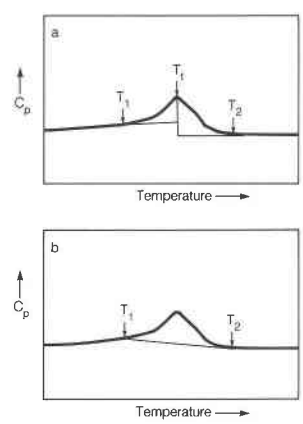

Fig. 3. (a) A schematic illustration of the calculation of ΔH_{trans} using Equation 3. The maximum point in the C_P curve is assigned to a temperature T_t. The points of tangency between the transition peak and the extrapolated C_P equations below and above the transition define the beginning and end transition temperatures, T_1 and T_2. Two integrations are performed from T_2 to T_t and T_t to T_1 to calculate ΔH_{trans}. (b) A schematic illustration of the calculation of ΔH_{trans} using Equation 4 in the text. A straight line is interpolated between T_1 and T_2 and defines the vibrational C_P, which is subtracted during a single integration.

Table 3. Transition temperatures

Sample No.	T_l (K)	T_h (K)	T_{h2} (K)	T_c (K)	T_{c2} (K)	T_2 (K)	Hysteresis (K)	ΔT (K)
89-21	760.0	864.0	877.0	855.0	868.0	920.0	9.0	160.0
89-21-A	756.0	840.0	857.0	833.0	850.0	878.5	7.0	122.5
90-05	763.5	885.5	906.5	876.5	898.0	927.0	9.0	163.0
SL.1	800.0	918.0	946.0	904.0	932.0	976.0	14.0	176.0
FL.1	757.0	823.5	-	807.5	-	839.5	16.0	82.5
SL.2	751.0	841.5	858.0	817.0	842.0	900.5	24.5	149.5
O1[1]	660.0	695.0	-	687.0	-	740.0	8.0	80.0
O1[2]	780.0	817.0	-	812.0	-	835.0	5.0	55.0
α−KF	650.0	729.5	-	720.0	-	830.0	9.5	180.0

T_l -- temperature at which the transition begins
T_h -- temperature at peak of C_p curve upon heating
T_{h2} -- temperature at secondary peak upon heating
T_c -- temperature at peak of C_p curve upon cooling
T_{c2} -- temperature at secondary peak upon cooling
T_2 -- temperature at which the transition ends
Hysteresis -- difference in temperature between T_h and T_c
ΔT -- temperature interval over which the transition occurs

[1]First transition at 695 K
[2]Second transition at 817 K

peratures were chosen. The two temperatures associated with the onset of a transition and its completion were determined by finding the points of tangency between the transition peak and the heat-capacity curves both below and above the transition (Fig. 3a). To determine what effect the rate of heating has on these data, samples were heated at 5 deg/min and 40 deg/min. Neither produced any significant difference in the temperatures of transition from samples heated at 20 deg/min. However, samples heated at 0.3 deg/min have transition temperatures that are approximately 3 to 4 deg lower than samples heated at the faster rates.

Heat-capacity data were fitted using standard regression procedures. Data points corresponding to temperatures below the transition were fitted to a three-term Maier-Kelley equation of the form $C_p = a + bT + cT^{-2}$. The limited number of data points corresponding to temperatures above the transition, up to 1000 K (DSC upper limit), were best fitted to the linear equation $C_P = a + bT$. Table 4 compiles the fit parameters of *a*, *b*, and *c* for each specimen. Calculated molar thermodynamic properties (enthalpy, entropy, heat capacity, and free energy) between 300 and 1000 K based on fit C_P equations from the experimental data are available upon request[1] for each of the ten samples listed in Table 1. Appendix Tables 1–4 tabulate experimental heat capacities for FL.1, synthetic leucite (SL.1), natural leucite (89-21), and O1.

Enthalpy and entropy of transition

Differential scanning calorimetry allows direct and highly precise measurements of heat capacity to be made over a continuous temperature interval. Integration of this heat-capacity data over any temperature interval provides the total change of enthalpy of the material:

$$\Delta H = \int_{T_1}^{T_2} C_P \, dT. \tag{1}$$

Integration of heat capacity divided by temperature provides the change of entropy:

$$\Delta S = \int_{T_1}^{T_2} C_P/T \, dT. \tag{2}$$

For some purposes, such as phase-equilibrium calculations at high temperatures, it may be sufficient to know the enthalpy and entropy of a mineral above its transitions. Calculations are made convenient by choosing a single transition temperature T_t, usually the peak in C_P, and deriving ΔH and ΔS of the transition by subtracting the extrapolated heat capacity ($C_{P,\text{extrap}}$) of the low-temperature phase below T_t and that of the high-temperature phase above T_t. Equation 1 becomes

$$\Delta H_{\text{trans}} = \int_{T_1}^{T_t} (C_{P,\text{obs}} - C_{P,\text{extrap}}) \, dT + \int_{T_t}^{T_2} (C_{P,\text{obs}} - C_{P,\text{extrap}}) \, dT. \tag{3}$$

A similar calculation is made for ΔS_{trans}. Here, T_1 and T_2 are the temperatures between which transition behavior is observed and are chosen as discussed above. Calculations show that a change of 10 deg in the assignment of the beginning or end transition temperature effects our calculated values of ΔH and ΔS by approximately 4%. An

[1] To obtain a copy of the thermodynamic data, order Document AM-86-309 from the Business Office, Mineralogical Society of America, 1625 I Street, N.W., Suite 414, Washington, D.C. 20006. Please remit $5.00 in advance for the microfiche.

Table 4. Fitted heat-capacity parameters

Sample	T_{range}(K)	a	b × 10^2	c × 10^{-5}	S.E.E.[2]
89-21	410-760	196.4	7.515	-55.17	.48%
89-21	920-999	224.8	1.063	-	.42%
89-21-A	410-756	163.2	11.5	-28.28	.23%
89-21-A	900-999	230.2	.6436	-	.34%
90-05	410-763	196.7	7.256	-56.81	.10%
90-05	940-999	226.1	1.052	-	.39%
1774	410-872	207.1	4.808	-66.82	.19%
SL.1	410-800	162.5	11.13	-23.35	.36%
FL.1	410-756	173.1	10.65	-24.87	.23%
FL.1	848-999	242.6	.1906	-	.26%
SL.2	410-751	184.3	9.080	-48.20	.20%
SL.2	910-999	236.2	.3440	-	.25%
O1	410-630	19.06	21.15	62.70	1.1%
α−KF	410-640	24.97	20.95	71.04	.42%
α−KF	850-999	147.7	4.000	-10.07	.18%
β−KF	410-999	158.0	2.838	-37.18	.46%

[1]Fit parameters to the Maier-Kelley equation: $C_p = a + b + cT^{-2}$ (J / gfw K)

[2]S.E.E. -- standard error of estimate of C_p

gfw -- gram formula weight based on six oxygens for leucites and four oxygens for O1, α-KF and β-KF

Table 5. Changes in enthalpy and entropy at transitions

Sample No.	[1]ΔH (J/gfw)	[2]ΔS (J/gfw K)	[3]ΔH (J/gfw)	[4]ΔS (J/gfw K)
89-21	2,862	3.311	3,383	3.972
89-21-A	2,629	3.109	3,006	3.614
90-05	2,851	3.220	3,719	4.275
SL.1	-	-	3,813	4.225
FL.1	2,049	2.416	2,433	2.989
SL.2	2,010	2.812	2,905	3.486
O1 [5]	-	-	597	0.797
O1 [6]	-	-	427	0.528
α−KF	-	-	933	1.280

[1]ΔH -- change in enthalpy using method shown in Figure 3a. [Eq. (3) in text.]
[2]ΔS -- change in entropy using method shown in Figure 3a.
[3]ΔH -- change in enthalpy using method shown in Figure 3b. [Eq. (4) in text.]
[4]ΔS -- change in entropy using method shown in Figure 3b.
[5]First transition at 695 K
[6]Second transition at 817 K
gfw -- gram formula weight based on six oxygens for leucites and four oxygens for O1 and α-KF

*The transition in SL.1 extends to the upper limit of the DSC and a fit equation for C_p above the transition is not possible. This precludes the use of Equation (3) to calculate ΔH_{trans}. For the O1 and α-KF specimens, extrapolation of C_p above and below the transitions produces an essentially straight line and thus only Equation (4) is used to calculate ΔH_{trans} and ΔS_{trans}.

illustration of this method is shown in Figure 3a, and results are included in Table 5.

This method, however, ignores the continuous nature of the transition that is spread over a broad range of temperature. The heat absorbed during this reversible transition between tetragonal leucite and cubic leucite cannot be assigned to a single temperature. Therefore, we present an alternative method for calculating the ΔH and ΔS of a transition that is still approximate and somewhat arbitrary, but takes into account its continuous nature. The simplest assumption, in light of our ignorance about the vibrational C_P during the transition, is to interpolate a straight line beneath the transition peak from T_1 to T_2 ($C_{P,\text{interp}}$; Fig. 3b) and use it to define the C_P, which is subtracted during a single integration:

$$\Delta H_{\text{trans}} = \int_{T_1}^{T_2} (C_{P,\text{obs}} - C_{P,\text{interp}})\, dT. \qquad (4)$$

Table 5 lists the results of both methods. The second approach leads to values of ΔH and ΔS that are consistently larger by 10 to 30%. Neither method is entirely satisfactory: the subtracted value in Equation 4, for example, may show a decrease in C_P with temperature over the transition interval. The difference between the two methods serves best to point out the uncertainties in estimates of ΔH_{trans} and ΔS_{trans} for a transition which is spread over a temperature range.

These results indicate that the ΔH and ΔS of transition for each leucite sample is strongly dependent upon the temperature of transition (Fig. 4). Those samples with higher transition temperatures have greater ΔH and ΔS values. Also, samples with similar transition temperatures have enthalpy and entropy changes that are also similar, especially within the uncertainty of the integrations. Additionally, the data show that the sum of the enthalpy changes for the two transitions in O1 is close to the value calculated for the single transition in orthorhombic $KFeSiO_4$ (α-KF).

Discussion

Leucite

The double-peaked nature of the heat-capacity curve during the transition in the natural and synthetic leucites suggests two structural events during the transformation from tetragonal to cubic symmetry. The two events are either related to two types of domains within the leucite crystal structure, each of which inverts to the cubic phase at different temperatures, or they are related to two transitions in which the whole structure undergoes two respective changes in symmetry (such as $I4_1/a$ to $I4_1/acd$ to $I3ad$). The latter interpretation implies that leucite has two tetragonal phases with different space groups ($I4_1/a$

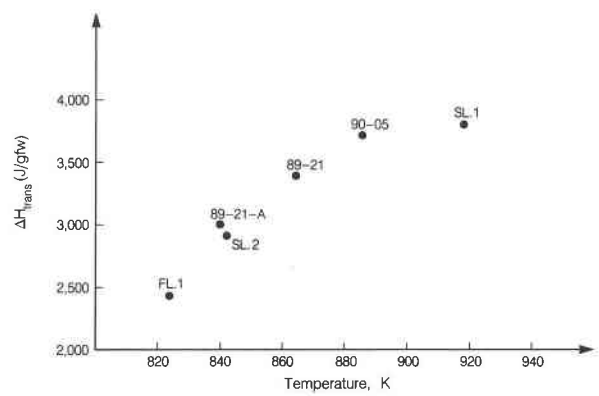

Fig. 4. The ΔH_{trans} for each specimen is plotted against its transition temperature (T_h, Table 3). Increases in transition temperatures can be correlated to greater ΔH of transitions.

and $I4_1/acd$). It is possible that different twin mechanisms are associated with the proposed cubic–tetragonal$_1$ and tetragonal$_1$–tetragonal$_2$ transitions, which explains the two types of twinning found in leucite (merohedric and pseudomerohedric; Mazzi et al., 1976). The twin planes for either of these twin mechanisms may form at domain boundaries. Evidence of a domain structure at high temperature is demonstrated by the "memory" effect (Mazzi et al., 1976) found in twinned leucites. When a twinned leucite crystal is heated to its cubic form and then cooled, the twinned crystal has the same proportion of twin domains with the same previous twin boundaries (Peacor, 1968; Sadanaga and Ozawa, 1968; Mazzi et al., 1976).

The leucites are also characterized by a broad transition temperature interval that could be related to a coexistence of phases. Henderson (1981) has presented high-temperature X-ray data indicating that SiO_2-rich natural leucites from the Leucite Hills, Wyoming (Carmichael, 1967), and the leucite-orthoclase solid-solution series ($KAlSi_2O_6$-$KAlSi_3O_8$) (MacKenzie et al., 1974) are characterized by a coexistence of two phases, one tetragonal and one cubic, during the tetragonal–cubic transition. A coexistence of two phases during a transition has been documented in several other framework silicate, aluminosilicate, and aluminate structures: the α–β transition in cristobalite (Leadbetter and Wright, 1976), the tetragonal–cubic transition in the solid-solution series $(K,Cs)AlSi_2O_6$-$(K,Rb)AlSi_2O_6$ (Martin and Legache, 1975), and the monoclinic–hexagonal transition in $(Sr,Ba)Al_2O_4$ (Henderson and Taylor, 1982).

One explanation for a coexistence of two phases during a transition involves martensitic-like behavior (Henderson and Taylor, 1982). Henderson and Taylor have suggested that volume discontinuity and anisotropy of shape between a transformed nucleus and its host crystal generates elastic strain that opposes the progress of transformation. Increases in temperature are necessary to provide sufficient energy for the transformation to proceed further. Thus, a broad interval of temperature (during which time both the transformed nuclei and the host phase coexist) is required to transform the whole crystal. The volume difference between tetragonal leucite and cubic leucite makes leucite eligible for this type of transformation.

The above explanation supports our contention that the tetragonal–cubic transition in leucite recorded on our C_P curves occurred near equilibrium conditions, although the transition is spread out in temperature. It is significant that after heat treatment for one week at 1673 K, sample 89-21-A has a more distinct second peak on the C_P curve and a transition event that is lower by 24 deg (Fig. 1d). The fact that prolonged heating above the transition temperature affects the nature of the transition is further evidence for a domain structure in the cubic phase (first indicated by the "memory" effect in twinned leucite described earlier).

The sharp resolution of two peaks on the C_P curve for sample 89-21-A suggests that an intermediate phase exists that is stable over approximately 17 deg (Fig. 1d). The proposed space group for the intermediate phase, $I4_1/acd$, can be related to the low-temperature tetragonal leucite phase ($I4_1/a$) by merohedric twinning and to the high-temperature cubic leucite phase ($Ia3d$) by pseudomerohedric twinning. According to Mazzi et al. (1976), merohedric twins develop on the tetragonal planes (110) and ($\bar{1}10$) with twinned structures having exactly parallel crystallographic orientations, but with the a and b axes interchanged. X-ray diffraction gives hkl diffractions of one twin exactly superimposed with khl diffractions of the other. The two individuals of the twin show simultaneous extinctions under crossed nicols, and the crystal appears optically to be without twinning. In contrast, pseudomerohedric twinning develops on the (101) (011) ($\bar{1}01$) ($0\bar{1}1$) tetragonal planes and creates twins with parallel a or b axes whereas the remaining pair of axes are not parallel. Thus, the individual twins have distinct spots in X-ray photographs and do not extinguish simultaneously when viewed under crossed nicols. It is this type of twinning in leucite with which petrographers are most familiar.

The single thermodynamic process involved with the transition in $KFeSi_2O_6$ is in marked contrast to the behavior of the aluminous samples. The failure of $KFeSi_2O_6$ to show a double set of peaks and hence, as we have implied, an intermediate tetragonal phase, may arise from a lack of Fe^{3+}-Si^{4+} disorder. Owing to the difference in their ionic size, Fe-Si disorder cannot easily take place in $KFeSi_2O_6$ (Faust, 1963). In contrast, leucite is completely disordered with respect to Al and Si in both the tetragonal and cubic phases (Peacor, 1968; Mazzi et al., 1976). Fe-Si order in $KFeSi_2O_6$ may preclude the stability of an intermediate tetragonal phase.

The C_P heating curve for the wyomingite leucite (Fig. 1e) lacks a peak yet does record a distinct, though small, increase in C_P at 900 K that continues to the upper limit of the DSC (1000 K). The apparent absence of twinning when viewed optically indicates suboptical pseudomerohedric twinning since the X-ray data shows it to be tetragonal. Because of the difficulty of obtaining a pure mineral separate from the wyomingite groundmass, the leucite sample is diluted by as much as 30% with other groundmass constituents which affect the size of the recorded peak.

$KAlSiO_4$ and $KFeSiO_4$

The transitions occurring in the orthorhombic forms of $KAlSiO_4$ and $KFeSiO_4$ may be similar to the multiple, displacive transitions in tridymite and subpotassic nephelines (Nukui et al., 1978; Thompson and Wennemer, 1979; Henderson and Roux, 1977; Henderson and Thompson 1980). The various phases along the join $KAlSiO_4$-$NaAlSiO_4$ are stuffed derivatives of the tridymite framework structure. Henderson and Thompson (1980) related the transitions occurring in these phases to various degrees of framework collapse. Tridymite is the archetypal mineral phase for the $NaAlSiO_4$-$KAlSiO_4$ system and undergoes four displacive transitions below 700 K (Thompson and Wennemer, 1979). DSC data on a pure-Na nepheline

synthesized by Henderson and Thompson (1980) indicate that it undergoes two transitions below 480 K which are separated by 20 to 40 deg. Their X-ray data show that the sample consists of two phases, one with an orthorhombic $3c$ superstructure and a second phase with even lower symmetry. Henderson and Thompson attributed the two transitions to the respective inversions of the two coexisting phases to hexagonal symmetry at different temperatures.

Our DSC results show that O1 undergoes one relatively rapid, reversible transition at 695 K and another at 817 K. The single transition observed by Pankratz (1968) for the sample referred to as synthetic kaliophilite corresponds to the second transition in O1 at 817 K. The two transitions in O1 either correspond to two coexisting phases (or domains) inverting to hexagonal symmetry at different temperatures [as suggested by Henderson and Thompson (1980) for their pure-Na nepheline] or to a single phase undergoing two changes in symmetry (similar to the multiple transitions in tridymite).

On the basis of the evidence of Cook et al. (1977) for two modifications of orthorhombic $KAlSiO_4$, it is conceivable that the first transition at 695 K is related to a symmetry change between two orthorhombic structures. However, the second transition at 817 K, observed in both O1 and Pankratz' sample, would then correspond to an orthorhombic–hexagonal transition. This type of transition is precluded by the fact that Pankratz identified his sample (below 817 K) as hexagonal synthetic kaliophilite (which has an X-ray pattern sufficiently different from orthorhombic $KAlSiO_4$ to make misidentification of the phase unlikely) and observed only a single transition at 817 K. Slight differences in synthesis conditions and composition may account for our synthesis of O1 vs. Pankratz' synthesis of kaliophilite. Alternatively, the C_P peak at 695 K could be related to a transition from O1 to a phase similar to hexagonal kaliophilite. The second peak would then represent the inversion of kaliophilite to an even higher hexagonal symmetry.

The orthorhombic form of $KFeSiO_4$ (α-KF) has a single transition spanning approximately 180 deg. Whether this transition is analogous to either the first or both transitions in O1 is uncertain. According to Bentzen (1983), a comparison of the orthorhombic $KFeSiO_4$ powder-diffraction pattern with those of the two modifications of orthorhombic $KAlSiO_4$ does not indicate isomorphism between the Fe and Al analogues although comparison of the unit-cell parameters suggests structural similarities. Energetically, the data indicate that the enthalpy and entropy of the transition in α-KF is approximately equivalent to that of the sum of the two transitions in O1. This result suggests that the transition in α-KF involves structural rearrangements that have been separated into two events in the O1 polymorph.

Conclusions

Four major conclusions have been drawn from the DSC data on natural and synthetic samples of leucite: (1) The broad transition temperature intervals in leucite may reflect a coexistence of phases during the transition and not disequilibrium conditions. (2) Heat treatment of a natural leucite (89-21-A) for one week at 1673 K sharpens the tetragonal–cubic transition into two distinct events. The separation of two peaks on the C_P curve (Fig. 1d) points to the existence of an intermediate phase that is stable over approximately 17 deg. (3) The intermediate phase can be assigned to the space group $I4_1/acd$ on the basis of the occurrence of two forms of twinning in leucite: merohedric and pseudomerohedric. Merohedric twinning can transform the tetragonal space group $I4_1/acd$ to $I4_1/a$ (low-temperature tetragonal leucite; Mazzi et al., 1976) whereas pseudomerohedric twinning can transform the cubic space group $Ia3d$ (high-temperature cubic leucite; Pankratz, 1968) to $I4_1/acd$. (4) The effect of Fe^{3+} substituting for Al in the leucite structure is to lower the tetragonal–cubic transition by at least 40 deg and to produce a single, sharp C_P peak (Fig. 1a). The Fe-Si order in $KFeSi_2O_6$ (Faust, 1963) is in contrast to the complete Al-Si disorder in leucite (Peacor, 1968; Mazzi et al., 1976) and may preclude the stability of an intermediate tetragonal phase.

The following observations have been made from the DSC data on synthetic samples of $KAlSiO_4$ and $KFeSiO_4$: O1 is characterized by one transition at 695 K and another at 817 K. At 695 K, the transition is from orthorhombic O1 to hexagonal kaliophilite, and the transition at 817 K transforms the phase to an even higher hexagonal symmetry. The orthorhombic iron analogue, α-KF, has a single transition at 729.5 K. The enthalpy and entropy data indicate that the single transition in α-KF is approximately equivalent to the sum of the two transitions in O1. Hexagonal β-KF ($KFeSiO_4$) undergoes no transitions below 1000 K.

Acknowledgments

We are grateful to Bruce Hemingway and Richard Abbott for critical reviews of the manuscript. This work was supported by the Director, Office of Basic Energy Sciences, Division of Engineering, Mathematics, and Geosciences, U.S. Department of Energy under contract DEAC03-76SF00098.

References

Abbott, R.N., Jr. (1984) $KAlSiO_4$ stuffed derivatives of tridymite: Phase relationships. American Mineralogist, 69, 449–457.

Bannister, F.A. (1931) A chemical, optical and X-ray study of nepheline and kaliophilite. Mineralogical Magazine, 22, 569–608.

Bentzen, J.J. (1983) Three crystalline polymorphs of $KFeSiO_4$, potassium ferrisilicate. American Ceramic Society Journal, 66, 475–479.

Carmichael, I.S.E. (1967) The mineralogy and petrology of the volcanic rocks from the Leucite Hills, Wyoming. Contributions to Mineralogy and Petrology, 15, 24–66.

Cook, L.P., Roth, R.S., Parker, H.S., and Negas, T. (1977) The system K_2O-Al_2O_3-SiO_2. Part 1. Phases on the $KAlSi_4$-$KAlO_2$ join. American Mineralogist, 62, 1180–1190.

Faust, G.T. (1963) Phase transition in synthetic and natural leucite. Schweizerische Mineralogische und Petrographische Mitteilungen, 43, 165–195.

Hamilton, D.L., and Henderson, C.M.B. (1968) The preparation

of silicate compositions by a gelling method. Mineralogical Magazine, 36, 832–838.
Henderson, C.M.B. (1981) The tetragonal–cubic inversion in leucite solid solutions. Progress in Experimental Petrology, 5, 51–55.
Henderson, C.M.B., and Roux, J. (1977) Inversions in sub-potassic nephelines. Contributions to Mineralogy and Petrology, 61, 279–298.
Henderson, C.M.B., and Taylor, D. (1982) The structural behavior of the nepheline family: (1) Sr and Ba aluminates (MAl_2O_4). Mineralogical Magazine, 45, 111–127.
Henderson, C.M.B., and Thompson, A.B. (1980) The low-temperature inversion in sub-potassic nephelines. American Mineralogist, 65, 970–980.
Hirao, K., Soga, N., and Kunugi, M. (1976) Thermal expansion and structure of leucite-type compounds. Journal of Physical Chemistry, 80, 1612–1616.
Holmes, A. (1942) A suite of volcanic rocks from south-west Uganda containing kalsilite (a polymorph of $KAlSiO_4$). Mineralogical Magazine, 26, 197–217.
Kelley, K.K., Todd, S.S., Orr, R.L., King, E.G., and Bonnickson, K.R. (1953) Thermodynamic properties of sodium-aluminum and potassium-aluminum silicates. Bureau of Mines Report of Investigation 4955, 1–25.
Leadbetter, A.J., and Wright, A.F. (1976) The alpha–beta transition in the cristobalite phases of SiO_2 and $AlPO_4$. I. X-ray studies. Philosophical Magazine, 33, 105–112.
MacKenzie, W.S., Richardson, D.M., and Wood, B.J. (1974) Solid solution of SiO_2 in leucite. Bulletin de la Société française de Minéralogie et de Cristallographie, 97, 257–260.
Martin, R.F., and Legache, M. (1975) Cell edges and infrared spectra of synthetic leucites and pollucites in the system $KAlSi_2O_6$-$RbAlSi_2O_6$-$CsAlSi_2O_6$. Canadian Mineralogist, 13, 275–281.
Mazzi, F., Galli, E., and Gottardi, G. (1976) The crystal structure of tetragonal leucite. American Mineralogist, 61, 108–115.
Nukui, A., Hiromoto, N., and Masaru, A. (1978) Thermal changes in monoclinic tridymite. American Mineralogist, 63, 1252–1259.
Pankratz, L.B. (1968) High-temperature heat contents and entropies of dehydrated analcite, kaliophilite and leucite. Bureau of Mines Report of Investigation 7073, 1–8.
Peacor, D.R. (1968) A high-temperature single-crystal diffractometer study of leucite $(K,Na)AlSi_2O_6$. Zeitschrift für Kristallographie, 127, 213–224.
Sadanaga, R., and Ozawa, T. (1968) Thermal transition of leucite. Mineralogical Journal, 5, 321–333.
Smith, J.V., and Tuttle, O.F. (1957) The nepheline-kalsilite system: I. X-ray data for the crystalline phases. American Journal of Science, 255, 282–305.
Stebbins, J.F., Weill, D.F., and Carmichael, I.S.E. (1982) High temperature heat contents and heat capacities of liquids and glasses in the system $NaAlSi_3O_8$-$CaAlSi_3O_8$. Contributions to Mineralogy and Petrology, 80, 276–284.
Taylor, D., and Henderson, C.M.B. (1968) The thermal expansion of the leucite group of minerals. American Mineralogist, 53, 1476–1489.
Thompson, A.B., and Wennemer, M. (1979) Heat capacities and inversions in tridymite, cristobalite, and tridymite-cristobalite mixed phases. American Mineralogist, 64, 1018–1026.
Tuttle, O.F., and Smith, J.V. (1958) The nepheline-kalsilite system. II. Phase relations. American Journal of Science, 256, 571–589.

Manuscript received May 6, 1985
Manuscript accepted March 18, 1986

App. Table 1. Experimental heat capacities of 89-21 (natural leucite)

Temp (K)	Heat Capacity (J/gfw K)	Temp (K)	Heat Capacity (J/gfw K)
420.0	197.4	845.0	274.7
450.0	203.4	850.0	281.5
500.0	212.1	855.0	291.5
550.0	218.5	860.0	304.7
600.0	224.9	865.0	310.3
650.0	231.3	870.0	300.5
700.0	238.2	875.0	289.5
750.0	245.0	880.0	280.2
760.0	246.6	885.0	267.2
765.0	247.2	890.0	252.5
770.0	248.3	895.0	245.4
775.0	249.0	900.0	241.5
780.0	250.0	905.0	238.9
785.0	251.1	910.0	237.4
790.0	252.3	915.0	236.0
795.0	251.4	920.0	234.9
800.0	252.5	950.0	233.6
805.0	253.8	990.0	237.0
810.0	254.9		
815.0	256.6		
820.0	258.5		
825.0	260.5		
830.0	263.2		
835.0	266.1		
840.0	269.8		

App. Table 2. Experimental heat capacities of SL.1 (synthetic leucite)

Temp (K)	Heat Capacity (J/gfw K)	Temp (K)	Heat Capacity (J/gfw K)
420.0	195.2	885.0	270.3
450.0	201.0	890.0	273.1
500.0	209.5	895.0	276.5
550.0	216.5	900.0	280.7
600.0	222.3	905.0	285.3
650.0	228.2	910.0	290.7
700.0	236.3	915.0	295.1
750.0	242.1	920.0	296.3
800.0	246.4	925.0	291.1
805.0	247.3	930.0	283.8
810.0	248.0	935.0	279.0
815.0	248.7	940.0	275.3
820.0	249.6	945.0	271.2
825.0	252.2	950.0	264.6
830.0	253.2	955.0	255.6
835.0	254.2	960.0	248.3
840.0	255.2	965.0	243.6
845.0	256.3	970.0	241.1
850.0	257.7	975.0	239.9
855.0	258.8	980.0	239.2
860.0	260.0	990.0	237.9
865.0	261.9		
870.0	263.4		
875.0	265.3		
880.0	267.6		

App. Table 3. Experimental heat capacities of FL.1

Temp (K)	Heat Capacity (J/gfw K)	Temp (K)	Heat Capacity (J/gfw K)
420.0	203.0	840.0	245.5
450.0	208.6	845.0	245.2
500.0	216.5	850.0	244.8
550.0	223.8	900.0	243.8
600.0	229.7	950.0	243.3
650.0	236.0	990.0	245.4
700.0	242.2		
750.0	249.5		
755.0	250.6		
760.0	251.5		
765.0	252.5		
770.0	253.7		
775.0	254.9		
780.0	256.5		
785.0	258.2		
790.0	260.1		
795.0	263.9		
800.0	268.0		
805.0	273.9		
810.0	288.0		
815.0	311.3		
820.0	375.6		
825.0	386.6		
830.0	252.2		
835.0	246.2		

App. Table 4. Experimental heat capacities of O1

Temp (K)	Heat Capacity (J/gfw K)	Temp (K)	Heat Capacity (J/gfw K)
420.0	140.9	770.0	173.4
450.0	145.2	780.0	173.7
500.0	151.8	785.0	174.2
550.0	157.2	790.0	176.2
600.0	161.9	795.0	177.4
650.0	169.2	800.0	179.7
660.0	172.4	805.0	184.0
665.0	169.1	810.0	191.5
670.0	170.5	815.0	202.5
675.0	172.5	820.0	195.2
680.0	175.6	825.0	178.5
685.0	180.1	830.0	176.9
690.0	187.0	835.0	176.6
695.0	192.8	840.0	176.6
700.0	188.1	850.0	176.9
705.0	181.3		
710.0	176.9		
715.0	174.6		
720.0	173.3		
725.0	172.7		
730.0	172.1		
735.0	172.0		
740.0	171.8		
750.0	171.7		
760.0	172.3		